

Analysis of Sub-Channel Correlation in Dual-Polarised MIMO Systems via a Polarisation Diversity Scheme

Cheng Fang, Enjie Liu, and Masood Ur Rehman

Abstract – A polarisation diversity combining scheme for dual-polarised Multiple-Input and Multiple-Output channels in small cell environments introduced and evaluated. The scheme is based on post analysis of channel measurement data captured from scenarios and includes indoor-to-indoor, indoor-to-outdoor, and indoor-outdoor-indoor propagation. An analysis of link signal strength and correlation with respect to frequency and polarisation revealed profound differences between co-polarised and cross-polarised links in terms of received signal strength and correlation between frequencies. Utilising these differences, a polarisation diversity combining scheme is evaluated which is shown to produce an average of 10.6dB polarisation diversity gain.

Index Term— Polarisation Diversity, MIMO, Correlation, Small Cells

I. INTRODUCTION AND BACKGROUND

In dual-polarised Multiple-Input and Multiple-Output (MIMO) channels, the sub-channels vary in terms of signal strength and correlation with respect to polarisation [1, 2]. This is especially true in small cell environments, where oblique reflections and scattering from indoor obstacles result in cross polarisation coupling, in which radio waves undergo changes in polarisation.

Antennas transmit signals according to their polarisation, and have best reception of signals whose polarisation matches their own; thus, the effects of polarisation can be seen at both ends of the link. At the transmitter, the signal power distributes on the surface of a sphere centred at the antenna, where the strength is related to the directions that are normal to the sphere. At the receiver, the power received will be related to both the strength and the polarisation of the arriving signal. If everything is aligned so the polarisation of an arriving signal is orthogonal to the receiving antenna, then the receiver will not pick up anything from that signal. In practice, a polarisation difference of 90° will result in an attenuation factor of 10 to 30 dB depending upon the equipment and the environment [3].

MIMO systems offer dramatic data throughput gains over SIMO systems [4], and their basic properties and advantages have been thoroughly investigated by many authors. It has been shown that the incident field and the far field of the diversity antenna obey an orthogonality relationship, and the role of mutual coupling is central [5], while comparisons between

spatial multiplexing schemes (SM) and diversity schemes via simulations revealed 6-12 dB higher SNR for diversity-based schemes, and 30-100% higher capacity for SM-based schemes [6]. Oestges et al. confirmed that average channel capacity in MIMO systems grows linearly with the number of antennas [7]. Colburn et al. [8] experimented on dual-antenna handsets which yield sufficient decorrelation for diversity systems, and Lo [9] studied the Maximal Ratio Transmission to be used for diversity on the transmission side. An overview of antenna selection in MIMO systems was presented by Sanayei & Nosratinia [10].

Exploiting the variations in signal strength and correlation from polarisation can lead to improved system performance for MIMO systems. In one of the earliest references to polarisation diversity, Lee & Yeh [11] demonstrated the feasibility of providing two diversity branches at UHF by polarisation diversity. Further, MIMO systems with partially correlated multipath fading can use polarisation diversity to provide a higher diversity gain [12], and diagonally correlated channels, for which dual-polarised channels constitute a highly practical scenario, have higher ergodic capacity than *independent and identically distributed* (i.i.d.) channels [13]. Nabar et al. [14] studied polarization diversity as a promising cost- and space-effective alternative to large antenna spacing often required in spatial diversity, while it was also shown that polarisation diversities can be exploited to increase the transmission performance of outdoor-to-indoor MIMO channels [15], and the channel capacity of indoor MIMO systems [16]. Dietrich et al. [17] examined the spatial and polarization diversity of wireless handsets and reported a diversity gain of 12dB to the SNR. Other related studies include an investigation into the effect of polarisation on the correlation and capacity of indoor MIMO channels [18]; a comparative study of channel capacities and MIMO correlation coefficient properties [19]; and the effects of antenna radiation patterns and multipath angular spread on the channel capacity [20].

In terms of data collection and modelling, outdoor MIMO propagation measurements carried out by Erceg et al. [21] at 2.48GHz using dual polarised antennas showed an estimated path loss exponent of 4.46, and a comparison between mono-polarised and dual-polarised Tx configurations at 2.5GHz revealed that a higher capacity can be achieved with the dual-polarisation antenna configuration, especially in the close-in range [22]. Quitin et al. [23] provides a closed-form solution for

determining the correlation coefficient and the XPD of a cross-polarised antenna; both correlation and XPD are shown to be sensitive to receiver orientation, azimuthal spread and environment depolarisation behaviour. The same authors also carried out a measurement campaign at 3.5 GHz to validate the analytical model [24], where the XPD of the wave is shown to be sensitive to spatial characteristics, while being insensitive to delay. Konishi et al. [25] found, for a small urban macrocell scenario at 4.5 GHz, that the cluster cross-polarisation ratios of MIMO channels were log-normally distributed, the HH polarisation path loss increased faster than VV with respect to distance, and the co-polarised gains were 4.65 dB higher than the cross-polarised gains.

However, there are other aspects of the effects of polarisation in MIMO systems that have not yet been thoroughly examined; for example, the small cells environment consists of various propagation scenarios including indoor-to-indoor (I2I), indoor-to-outdoor (I2O), outdoor-to-indoor (O2I), indoor-outdoor-indoor (IOI). Most existing research concentrates on only one of the scenarios. The data used in the research presented here includes measurements from all of these scenarios; the measurements were made using antenna arrays consisting of dual polarised elements at both ends of the transmission link, giving rise to four possible Tx-Rx polarisation combinations. In addition, due to the transmission bandwidth and antenna geometry, the data also allows for an analysis of polarisation effects in relation to sub-channel frequency and receiver orientation, leading to a systematic empirical study of the effects of polarisation in small cells MIMO systems.

This paper aims to detect and statistically characterise the systematic influences of antenna polarisation in small cells MIMO systems through empirical measurements, and to evaluate potential polarisation diversity schemes for such systems. The remainder of this paper is organised as follows. Section II describes the data collection campaign, including details of the experimental location, equipment, set-up and procedures, while Section III explains the basic considerations and methodologies of the data analysis. Section IV presents the main findings of the investigation, and Section V introduces and evaluates a potential polarisation diversity scheme based on the outcomes of Section IV. Section VI summarises the findings presented in the paper and provides further discussion.

II. DATA COLLECTION

A. Location

The measurements were carried out at Lund University (LTH), Sweden; more specifically, at the E-Huset of its Faculty of Engineering. The sections of the building in which the data collection took place are shaped in a way that allows indoor-indoor, indoor-to-outdoor, as well as indoor-outdoor-indoor measurements to be taken.

B. Equipment

A planar Tx array and a cylindrical Rx array were used. The Tx array consisted of 16 dual polarised patch antenna elements arranged in 2 rows \times 8 columns (only the middle 2 rows were active, as shown in Figure 1a), while the Rx array was made up

of 64 dual polarised patch elements arranged in 4 rows \times 16 columns (Figure 1b). Since all of the patch elements were dual-polarised, the result is a 128×32 MIMO system.

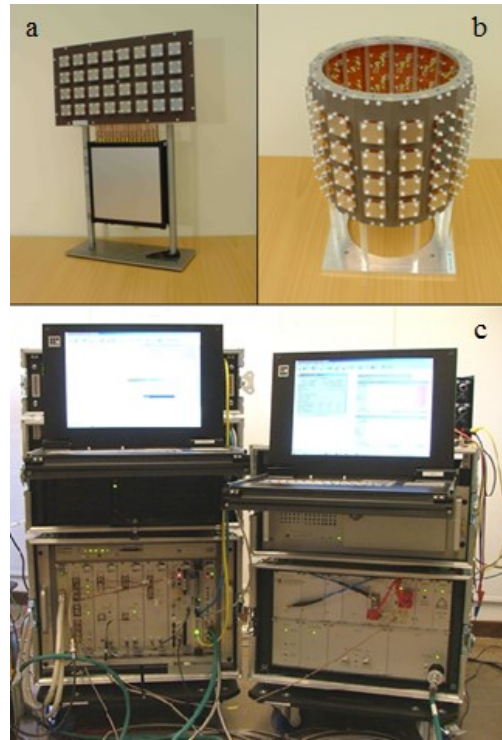


Figure 1: (a) Tx Array, (b) Rx Array, (c) RUSK LUND Channel Sounder

Using the RUSK LUND channel sounder [26, 27] (Figure 1c), the measurements were performed at a central frequency of 2.6 GHz, with a signal bandwidth of 50 MHz and a transmit power of 40dBm. The maximum measurable delay was 1.6 μ s. At the receiver, the transfer function was measured at 81 points in the frequency domain. The sampling time for a set of MIMO snapshots was 0.026s.

Five consecutive snapshots form one block, with no delay between the snapshots. There was a delay of 1s between each block. During the measurements, the Tx was fixed in a particular room, whilst the Rx was moved to different positions throughout the building and outdoors, see Figure 2 caption for more detailed explanation. Two blocks of data were recorded for each measurement position, thus providing 10 temporal snapshots.

Consequently, the data used in this study contains, at each measurement position, a channel transfer matrix with dimensions $10 \times 81 \times 4096$; the dimensions represent temporal snapshots, frequency samples, and individual MIMO links respectively. Both the Tx and Rx were static during the measurements, and the coherence time was quite large (160ms), as expected. The measurements were carried out during the summer holidays and there was on one in the Tx room and very few people moving about the building. The noise floor was consistently measured to be -102dBm.



Figure 2. Measurement positions: Rx positions are marked by dots, while Tx positions are marked by crosses; arrows indicate the direction in which Tx is facing.

III. METHODOLOGY

With dual polarised antenna elements in both Tx and Rx, there are four possible polarisation pairings, namely: VV, VH, HV and HH. The letters specify the polarisations of the receiver and transmitter elements, respectively. For example, HV represents a channel with a horizontally polarised receiver element and a vertically polarised transmitter element. Recall that at each measurement position, the data collected is in the form of a channel transfer matrix of dimensions $10 \times 81 \times 4096$. Since each of the four polarisation pairings accounts for exactly one quarter of the data, the transfer matrix can be split into 4 matrices, of dimension $10 \times 81 \times 1024$, each exclusively containing data of a specific polarisation pairing.

The objective is to investigate and characterise the effects of sub-channel polarisation with respect to frequency. For each one of the 81 frequencies there are 10×1024 matrix elements, which accounts for all of the data collected at a particular measurement position for one specific frequency and polarisation pair. Thus, at each measurement position, four polarisation specific matrices of dimension 10240×81 can be derived from the data; these are denoted by \mathbf{X}_{vv} , \mathbf{X}_{vh} , \mathbf{X}_{hh} , \mathbf{X}_{hv} , where the subscripts correspond to the polarisation pairing, they are referred as *polarisation matrices* in the rest of the paper.

Correlation analysis were performed on the polarisation matrices via comparison of frequency columns. The correlation between two column vectors was evaluated by the Pearson product-moment correlation coefficient [28]. In this approach, if \mathbf{U} and \mathbf{V} denote the two data vectors of length l , then the correlation coefficient, r , between \mathbf{U} and \mathbf{V} is calculated by:

$$r = \frac{\sum_{i=1}^l (u_i - \bar{u})(v_i - \bar{v})}{\sqrt{\sum_{i=1}^l (u_i - \bar{u})^2 \sum_{i=1}^l (v_i - \bar{v})^2}} \quad (1)$$

As mentioned before, four polarisation matrices are generated from one measurement position. If \mathbf{U} represents a column from polarisation matrix \mathbf{P}_1 and \mathbf{V} represents a column from polarisation matrix \mathbf{P}_2 , then a matrix \mathbf{E} can be constructed by computing the correlation coefficient r for all possible pairs of \mathbf{U} and \mathbf{V} drawn from \mathbf{P}_1 and \mathbf{P}_2 . When \mathbf{P}_1 and \mathbf{P}_2 represent the same polarisation matrix, \mathbf{E} is known as an autocorrelation matrix and will be symmetrical. There are four such autocorrelation matrices, one for each of the polarisation pairings:

$$(\text{VV}, \text{VV}), (\text{HH}, \text{HH}), (\text{VH}, \text{VH}), (\text{HV}, \text{HV})$$

When \mathbf{P}_1 and \mathbf{P}_2 are different correlation matrices, \mathbf{E} is known as cross-correlation matrix and it will not be symmetrical. There are 12 such cross-correlation matrices which consists of 6 pairs of matrices and their transposes. As it is unnecessary to repeat the correlation calculations for the transpose matrices, we are left with 6 pairs as shown below:

$$(\text{VV}, \text{VH}), (\text{VV}, \text{HV}), (\text{VV}, \text{HH})$$

$$(\text{VH}, \text{HV}), (\text{VH}, \text{HH}), (\text{HV}, \text{HH})$$

The correlation matrices will indicate whether the columns (each one being the complete collection of sample data of a particular polarisation and frequency) are related to each other. Observing and comparing data collected from the same measurement position is a direct way to reveal and evaluate any polarisation effects there might be. In addition, comparing the correlation patterns observed between data from different measurement positions is a way to gain a perspective on any existing polarisation effects that are consistent across different measurement positions. A practical approach for undertaking these comparisons is to investigate the correlation of correlation patterns. This can be more explicitly stated as the operation that firstly reshapes a correlation matrix into a vector by concatenating its columns, and then computing the correlation coefficients between two such vectors.

Because the correlation coefficient is estimated from sampled data, its value could potentially show small degrees of correlation by random chance. To make sure that any potential correlation is due to the inherent characteristics of the data rather than randomness, we need to test the significance of the estimated coefficient values. For this, the t -test [29] is used; it is based on the assumption that the data distribution is Normal. From the results obtained, it was found that the distribution of received signal power in Watts is approximately Lognormal, so it is reasonable to assume that the distribution of received signal strength in dBm will be approximately Normal. A description of the t -test method can be found in [30].

IV. POLARISATION EFFECTS ON SIGNAL STRENGTH AND CORRELATION

A. Signal Strength

The polarisation matrices \mathbf{X}_{vv} , \mathbf{X}_{vh} , \mathbf{X}_{hh} and \mathbf{X}_{hv} are of dimension 10240×81 . Their rows correspond to samples

obtained from different channels at various times, while the columns correspond to 81 frequency samples evenly distributed around 2.6GHz with a 50 MHz bandwidth. For any given column, the 10240 data points represent the complete sample of data collected from a particular measurement position under a specific combination of polarisation and frequency, i.e. it contains data from all individual links and all time delays.

Figure 3 shows a boxplot of the mean received signal strength of differently polarised links across the 81 frequencies, averaged across all measurement positions. The presence of polarisation effects can be clearly seen. Firstly, for co-polarised settings (VV and HH), the centres of power distributions across the frequency domain form an almost flat line, indicating that the signal strengths do not vary greatly across the frequency domain. In contrast, the mean received signal strength for VH and HV settings varies by as much as 12 dB across the frequency domain, with the variation pattern somewhat periodic. This periodic variation is the result of Polarisation Fading, which is caused by changes in the polarisation during the propagation of cross-polarised EM waves.

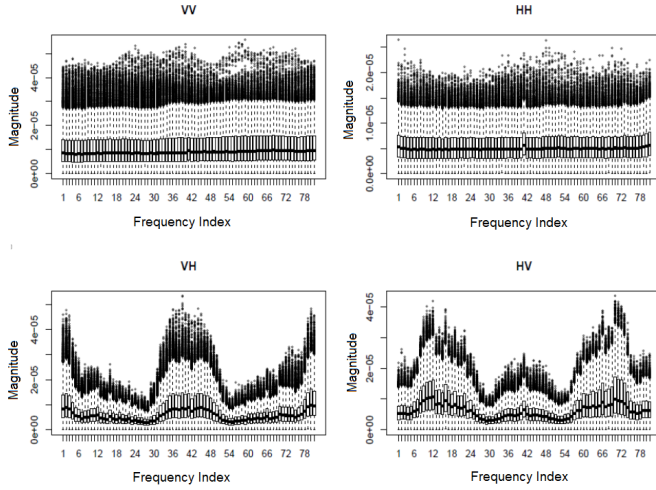


Figure 3. Signal power distribution of the 4 polarisation settings across 81 frequencies

Further, the co-polarised channels show very consistent quartiles, whereas the quartiles for cross-polarised channels are really narrow at certain frequencies and wide at others. Hence, polarisation has a considerable effect on the power distribution of the received signal. The consistency of co-polarised channels is helpful for prediction and planning. The periodic variations of signal strength in cross-polarised channels can also be utilised in beneficial ways by employing appropriate polarisation diversity schemes – for example, sub-channels with central frequencies located around distinct peaks can be picked out and these will have good reception and will experience less interference than normal around the intervening frequencies. This will be explored later in this paper.

To identify the existence of significant polarisation effects, we consider the mean received power from all measurement positions, spread across the frequency domain. This is shown in Figure 4. The mean received power is calculated as follows. At each measurement position, the channel sounder records complex frequency responses and generates a four-dimensional

channel transfer matrix $\mathbf{H}(t, f, i, j)$ in which the parameters are time, frequency, Rx and Tx indices, respectively. Using the *Inverse Fourier Transform*, \mathbf{H} is transformed into the channel impulse response matrix $\mathbf{h}(t, \tau, i, j)$, where τ denotes delay. This enables the instantaneous received power $\mathbf{P}(t, \tau, i, j)$ for the individual Rx_{*i*} - Tx_{*j*} link to be estimated, as below [31]:

$$\mathbf{P}(t, \tau, i, j) = |\mathbf{h}(t, \tau, i, j)|^2 \quad (2)$$

As in the case of the polarisation matrices, we consider each of the four polarisation states separately and introduce four vectors \mathbf{P}_{VV} , \mathbf{P}_{VH} , \mathbf{P}_{HV} and \mathbf{P}_{HH} which represent the received power at the given delay. The averaging takes place across antenna elements and temporal snapshots (i.e. the t , i and j dimensions), as below.

$$\begin{aligned} \bar{\mathbf{P}}_{VV}(\tau) &= \frac{1}{n_t n_i n_j} \sum_{t=1}^{n_t} \sum_{i=1}^{n_i} \sum_{j=1}^{n_j} \mathbf{P}_{VV}(t, \tau, i, j) \\ \bar{\mathbf{P}}_{VH}(\tau) &= \frac{1}{n_t n_i n_j} \sum_{t=1}^{n_t} \sum_{i=1}^{n_i} \sum_{j=1}^{n_j} \mathbf{P}_{VH}(t, \tau, i, j) \\ \bar{\mathbf{P}}_{HV}(\tau) &= \frac{1}{n_t n_i n_j} \sum_{t=1}^{n_t} \sum_{i=1}^{n_i} \sum_{j=1}^{n_j} \mathbf{P}_{HV}(t, \tau, i, j) \\ \bar{\mathbf{P}}_{HH}(\tau) &= \frac{1}{n_t n_i n_j} \sum_{t=1}^{n_t} \sum_{i=1}^{n_i} \sum_{j=1}^{n_j} \mathbf{P}_{HH}(t, \tau, i, j) \end{aligned} \quad (3)$$

The *Fourier Transform* is now applied to convert these vectors back into the frequency domain, in terms of dB

$$\bar{\mathbf{P}}_{VV\text{dB}}(f) = 10 \log_{10}(\bar{\mathbf{P}}_{VV}(f)) \quad \dots \quad (4)$$

Finally, the value of the noise floor is added to obtain the received power in dBm. This process is repeated at each measurement position and results are averaged to produce the control chart shown in Figure 4. In the figure, the horizontal lines are control lines: solid lines mark the central control lines, dotted lines mark the upper control lines and dashed lines mark the lower control lines. Both types of control lines are 0.01 probability limits. The four colours correspond to the different polarisation settings: red for VV, green for VH, orange for HH and black for HV. For a given polarisation, if the dispersion of the amplitude data is random, the corresponding sample means should be scattered between the upper and lower control lines. If any data points lie outside these boundaries, frequency associated dispersion will probably be the cause.

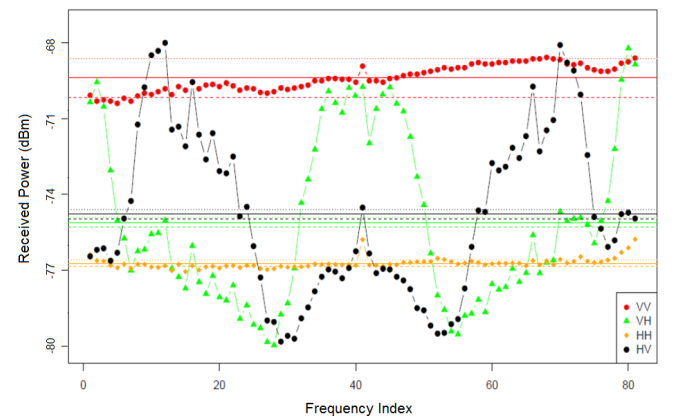


Figure 4. Variation of the mean received power across the frequency domain.

The figure shows that the co-polarised signals (HH and VV) are largely unaffected by frequency, whereas cross-polarised signals (HV and VH) are greatly affected. A major contributing factor to this discrepancy is polarisation fading, which is caused by co-polarised waves [32]. Moreover, Figure 4 shows that the peak signal strength for cross-polarised waves is higher than co-polarised waves, giving potential for polarisation diversity. Incidentally, polarisation fading is also reduced by polarisation diversity [32], thus polarisation diversity is of great interest and will be explored in section V.

Overall, the mean signal strength is highest for the VV waves and lowest for HH, with a difference of around 7 dB between the two. This is probably caused by a combination of low antenna heights, which typically results in stronger vertically polarised signals for the indoor environment [33], and Brewster's angle phenomenon, which affects the propagation of horizontally polarised waves in indoor environments [34].

It can be seen that the mean signal strengths for the HV and VH settings are very close, in fact within 0.1 dB of each other, despite the fact that their values differ by more than 3 dB over 75% of the frequency points. This is due to the periodical nature of the cross polarisation fading particular to the system. The HV and VH signals exhibit constructive and destructive interference and are out of phase with each other.

B. Signal Correlation

This sub-section presents the findings of the investigations into signal correlation. The correlation heat maps in Figure 5 and Figure 6 provide visual representations of the ten correlation matrices constructed from pairwise combinations of the four polarisation matrices. Both figures display data from a particular measurement position for the I2I group; the figures for all other measurement positions, including the I2O and IOI scenarios, exhibit very similar patterns. The extent of their similarity is analysed in Section IV.C.

The elements of the correlation matrices are real numbers between 0 and 1. Values close to 0 correspond to low levels of correlation and are shown in dark blue; values close to 1 represent high levels of correlation and are shown in dark red. The numbers on the axes indicate the frequency index. Note that the correlation coefficient between the same frequency columns of the same polarisation matrix is always 1, and the operation that computes the correlation coefficient between two columns is commutative. Thus the four autocorrelation matrices are always symmetrical, as can be seen in Figure 5.

The figure reveals a stark contrast between the correlation matrices of the co-polarised and cross-polarised settings. For the co-polarised settings, the strength of the correlation is relative to the perpendicular distance from the diagonal. Stripes parallel to the diagonal are of uniform 'potential' i.e. they contain correlation coefficients with very similar values. The value gradually decreases as the focus of observation moves away from the diagonal. The VV setting shows a significantly stronger correlation than the HH setting in the regions near the diagonal. This implies that VV polarisation setting would have a wider coherence bandwidth.

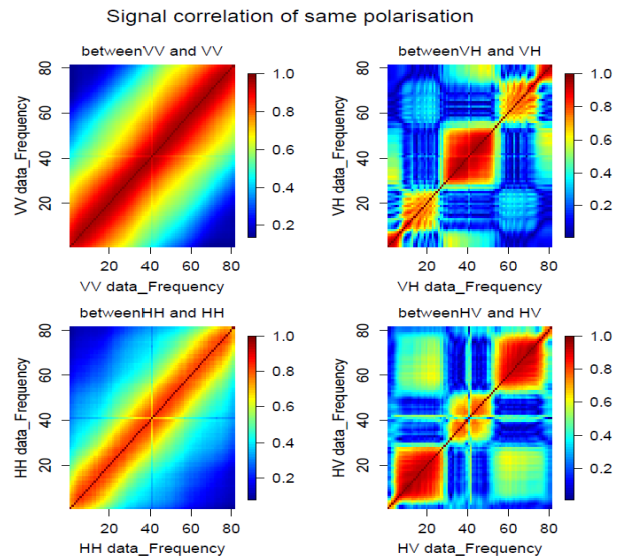


Figure 5. Heat map of signal correlation between the same polarisation settings

For the cross-polarised settings, the correlation heat maps present a chequered pattern; this is probably due to the polarisation fading effects particular to cross-polarised waves [32]. There are elements adjacent to the diagonal which are calculated from samples with only a 0.625 MHz frequency offset but the correlation coefficient is close to 0. The correlation patterns for VH and HV appear to match after a diagonal shift of roughly 20 frequency offsets, which equates to 12.5 MHz. The patterns for co-polarised settings are as expected, with the correlation being stronger near the diagonal where the frequency offset is small, and gradually becoming weaker as the frequency offset increases. The chequered correlation patterns for cross-polarised settings are of great interest as it appears to be a regular, periodic and predictable pattern. The fact that data from frequency samples so close to each other can have correlation close to 0 is also surprising. Here, the obvious explanation of low measurement SNR can be disregarded as it can be seen from Figure 4 that the weakest signal, at -80dBm, is still a good 20dBs stronger than the measured noise floor, which was -102dBm. This discrete pattern of correlation is readily exploitable as signals from certain widely separated frequency bands are highly correlated, thus reducing the requirement on the SINR threshold to maintain a wide channel. In other more closely packed bands, the signals are not correlated, which naturally helps with interference. Knowing these patterns will greatly help to improve the channel efficiency.

Moving onto Figure 6 which shows the correlation heat map for the 6 cross-correlation matrices. Looking at the patterns that emerged, these matrices can be split into 3 groups shown in the columns from left to right:

1. Those with the same Tx setting but different Rx settings: (VV, HV) and (VH, HH)
2. Those with the same Rx setting but different Tx settings: (VV, VH) and (HH, HV)
3. Those where the Tx and Rx settings are both different: (VV, HH) and (VH, HV)

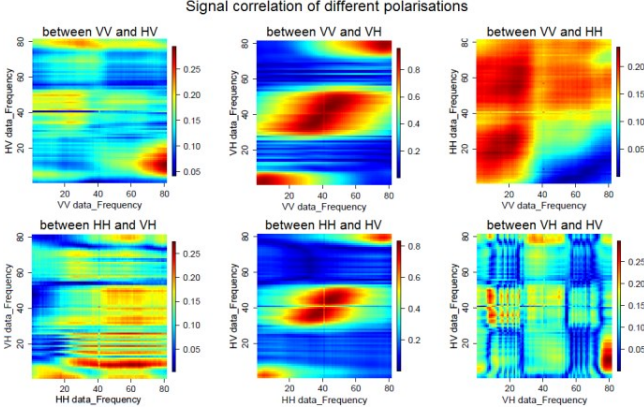


Figure 6. Heat map of signal correlation between different polarisation settings

The first thing to note is that the correlation in Group 2 is much stronger than in Groups 1 and 3. The correlation patterns in Group 1 are similar and form roughly equidistant stripes parallel to the co-polarised axis, which implies that the correlation varies periodically with respect to frequency for these cross-polarised settings whereas it stays roughly constant with respect to frequency in co-polarised settings. The patterns in Group 2 are also similar, and provide validation for each other, though the correlation is stronger for vertically polarised receivers. The patterns in Group 3 are very different, and it can be seen that the correlation between the two different co-polarised settings is much stronger than the corresponding correlation between the two separate cross-polarised settings.

Thus, the investigation into correlation has revealed that polarisation has a systematic effect on signal correlation in relation to frequency; instead of being a collection of random values, the correlation coefficients fall into highly structured patterns. Polarisation has significant effects on the signal correlation, with co-polarised settings exhibiting patterns that are vastly different from those of cross-polarised settings. Cross-polarised channels exhibit an interesting chequered pattern which can be utilised for increased channel efficiency.

C. Inter-site correlation of signal correlations from different measurement positions

In the previous sub-sections, the correlation matrices exhibited clear patterns, but the figures generated were from data collected at a single measuring position, which was selected as a typical representation. However, variations will be found when changing the positions, so we should not draw immediate conclusions based on their ‘typicality’. In this subsection, we therefore correlate the correlation patterns themselves; this is crucial for the validation of the findings of the previous sub-sections.

To assess if the patterns are specific to one position only, the correlations between the patterns of all 123 measurement positions were examined. This is possible because the information contained in the correlation matrices is arranged in a fixed order, and forms one-to-one correspondences with correlation matrices from other measuring positions. For example, column 5, row 16 of a frequency related amplitude correlation matrix from any measuring position would always contain the correlation coefficient between samples

corresponding to the 5th and the 16th frequency offsets measured at that position. With this fixed order, the correlation coefficients between the matrices from two different positions can be computed by rearranging both correlation matrices into vectors (by concatenating the columns) and computing the correlation coefficient between these two vectors as before.

Inter-site Correlation of Signal Correlation in Frequency Domain

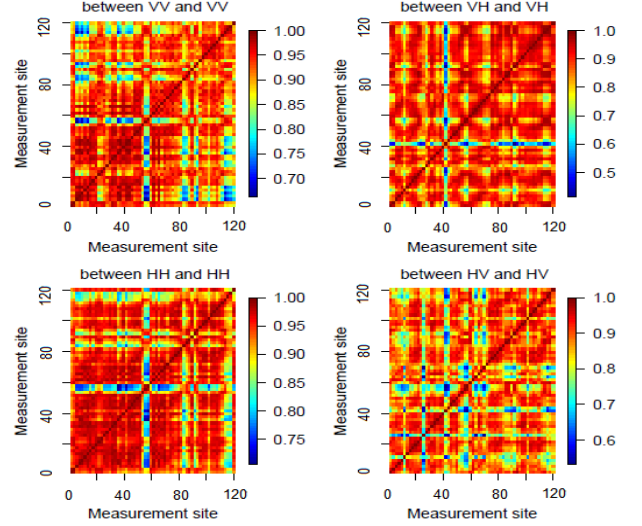


Figure 7. Correlation of signal correlation across measuring sites

Figure 7 shows the correlation of signal correlation matrices across all 123 measurement positions. The correlation patterns for cross-polarised settings are almost entirely red (correlation coefficient > 0.8), indicating high levels of correlation between all measuring positions. The patterns for co-polarised settings show a greater variation in the correlation value but, on the whole, they are still dominated by orange and red regions representing coefficient values over 0.7. This confirms that the individual site-specific signal correlation patterns are highly correlated across the different measuring positions, validating the conclusions drawn about the effect of polarisation on signal correlation in the previous sub-section.

In summary, the results presented in this sub-section confirm the consistency of the correlation patterns presented in the previous sections across all of the measuring sites and, in doing so, they validate the findings of previous sub-section.

V. POLARISATION DIVERSITY COMBINATION SCHEME

In our dual-polarised MIMO system, each Rx is either vertically polarised (V) or horizontally polarised (H), and receives multiple signals from differently polarised Tx’s which are also either V or H. This variance in polarisation can be taken advantage of through polarisation diversity.

Diversity Gain (DG) is a figure of merit to measure the improvement in signal quality achieved through application of diversity techniques, e.g. polarisation diversity in our case. It is an enhancement in a particular performance metric (e.g. signal strength, SNR, or BER) over a single antenna with no diversity, at a certain level of outage probability [5, 8]. The diversity gain is commonly calculated as the difference in the performance metric of the diversity combined signal and the strongest branch

signal (taken as a reference) among all the diversity branches, i.e.

$$DG \text{ (dB)} = P_{\text{div}} - P_s$$

where P_{div} is the power level of the diversity combined signal and P_s is the power level of the reference signal. In our case, the performance metric used is signal strength calculated from the channel sounder measurements, and the reference signal is the strongest signal at a certain frequency within each polarisation setting group.

Our MIMO system contains 32 Tx and 128 Rx, thus, each individual Rx receives 32 signals from different Tx. First, the 32 signals are combined using *Maximal-ratio Combining* (MRC), where the gain of each link is made proportional to the rms signal strength and inversely proportional to the noise. The signals are then added together with different proportionality constants attached to each. As a caveat, since the technique combines different Tx signals rather than Rx signals, the technical terms should be *Maximal-ratio Transmission* (MRT) [9]; however, the mathematical process is identical to MRC which is a better-known term. It is well established that the performance of MRC is greatly affected by signal correlation [35], so appropriate consideration has to be given in this regard. The findings from the previous section, as shown in Figure 5 and Figure 6, provide evidence that the signal correlation is affected by both frequency and polarisation, as the correlation between particularly polarised links are high at certain frequencies and low at others. This is a piece of useful knowledge as it allows us to appropriately weigh the frequencies to achieve the best performance for MRC. Once MRC has been individually carried out at all 128 Rx's, *Selection Combining* (SC) on the 128 post-MRC Rx signals is employed to obtain P_{div} . Figure 8 provides an illustration of the proposed diversity combination scheme.

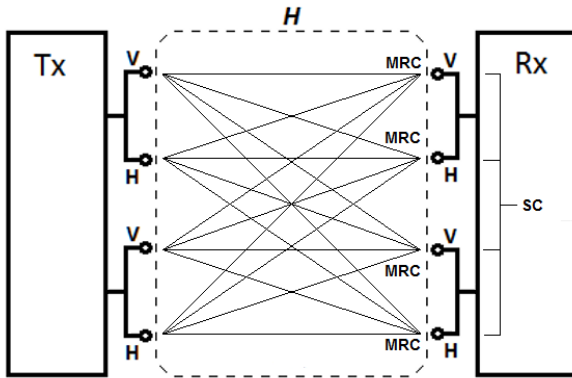


Figure 8. Polarisation diversity combination scheme for dual-polarised MIMO channel

Using the above combination scheme, the polarisation diversity gain against each of the four polarisation settings can be computed. Figure 9 shows a heat map of the diversity gain of P_{div} against four reference signals, which are the strongest signals within each polarisation group, across frequencies. The heat map is split into 4 sections corresponding to the four polarisation groups. Each corresponding row of a section represents data from one particular measurement position.

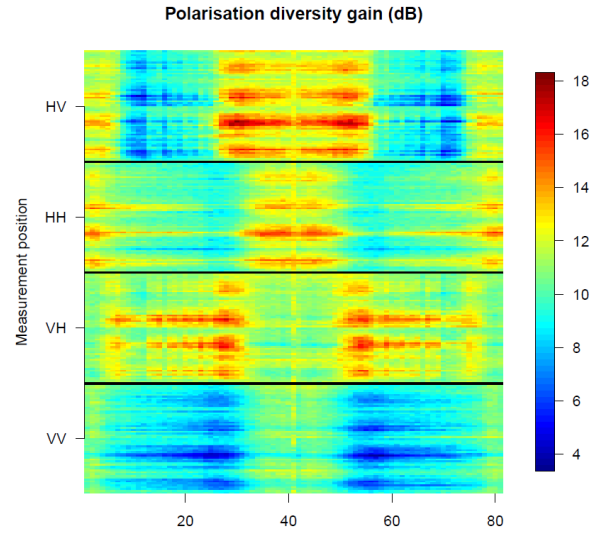


Figure 9. Polarisation diversity gain for each polarisation setting across different frequencies

The figure shows that diversity gain is also dependent upon the frequency, which is a consequence of the frequency selective behaviour of the polarisation fading exhibited in Figure 5. Furthermore, cross-polarised sub-channels (HV and VH) exhibit greater diversity gain than co-polarised channels, which is expected for the low 3dB [16] value of XPD for the (small cells) measurement environment. It is interesting to note that due to the periodic variation of sub-channel signal strength demonstrated by results from previous sections, the range of frequencies corresponding to the highest diversity gain is different for HV and VH. This is very useful and can be exploited by selecting the polarisation setting with the highest gains for each frequency.

Figure 10 shows the average polarisation diversity gain across all measurement positions for each of the four possible polarisation settings.

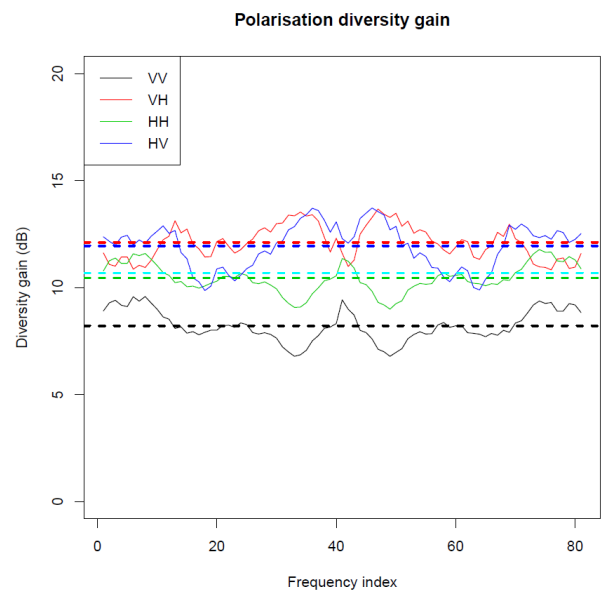


Figure 10. Mean polarisation diversity gain across all measurement positions for differently polarised sub-channels

The dotted lines, with colours corresponding to the legend, indicate the mean diversity gain after further averaging across frequencies. The cyan dotted line represents the overall mean diversity gain. As can be seen from the figure, the gains for cross-polarised sub-channels VH and HV are similar (12.2dB and 12.1dB, respectively) and significantly higher than for the co-polarised sub-channels – the gains for HH and VV are 10.4dB and 7.9dB, respectively. This is because previous results revealed that VV sub-channels have the highest signal strength and therefore the vertical component of the XPD, X_v , is the highest, which leads to lower diversity gains for VV. The overall mean polarisation diversity gain is 10.6dB.

Figure 11 shows histograms of raw channel power for differently polarised sub-channels in comparison to the power achieved after applying the proposed polarisation combination scheme shown in Figure 8. The figure displays data from one snapshot at one particular measurement position. As mentioned earlier, the channel transfer matrix measured in each position has dimensions $10 \times 81 \times 4096$ (snapshots \times frequencies \times MIMO links). The 4096 MIMO links are split into VV, VH, HV and HH Tx-Rx polarisation combinations hence each histogram in Figure 11 contains $81 \times 1024 = 82944$ sample points. By visual inspection, the application of polarisation diversity makes the distribution of channel power less skewed than individual polarisations; as a result, diversity gain is achieved.

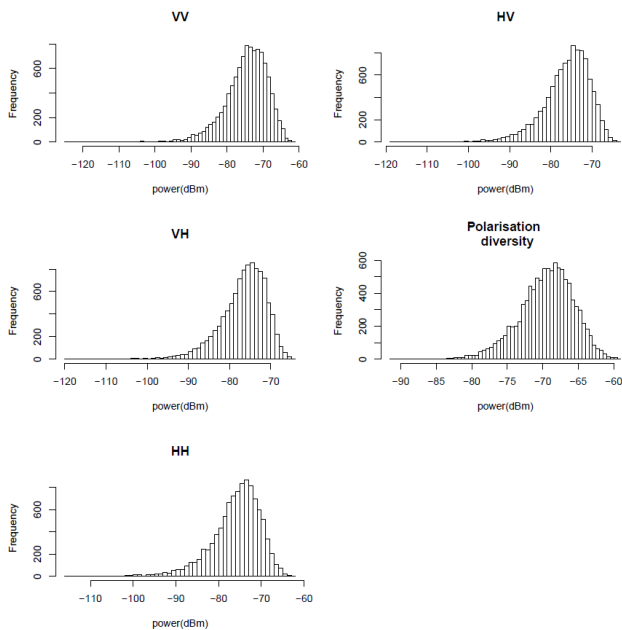


Figure 11. Histograms of the raw channel power for different polarisation settings in comparison with power achieved through the proposed diversity combining scheme

Figure 12 shows the CDF of the strongest branch signal strength within each individual polarisation setting in comparison with the polarisation diversity combined signal strength. The ordinate shows the probability that the channel power is smaller than the power on the corresponding abscissa. As can be seen, the polarisation diversity achieves a significant gain over individually polarised branches. The median, or 50th percentile, channel power from the diversity scheme is -67dB compared to -75 to -76dB for individual sub-channels.

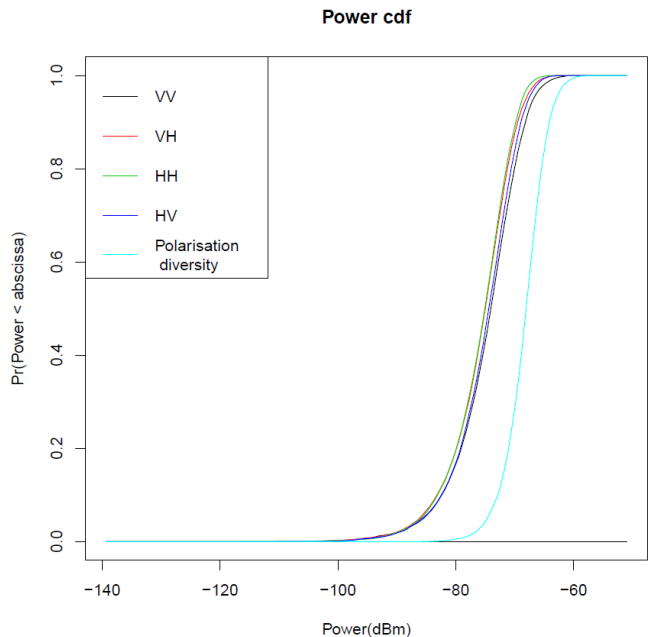


Figure 12: CDF of sub-channel power for different polarisation settings in comparison with polarisation diversity combining scheme

VI. CONCLUSION

This paper presented the effect of polarisation on sub-channel correlation in relation to frequency for dual-polarised MIMO channels in small cell environments. Polarisation settings have a significant effect on the strength of the received signal. The VV setting generally performed the best with mean received signal strength 7 dB higher than the lowest average HH. The signal strengths across the frequency domain are stable for co-polarised settings but for cross-polarised settings the signal strengths vary considerably by up to 12dB.

For cross-polarised settings, the variations in signal strength across the frequency domain display a periodic nature such that if the signal strength for HV is relatively high, then the signal strength for VH at the same frequency is relatively low, and vice versa. As a consequence, even though the received signal strength between the 2 cross-polarised settings differs by more than 3 dB at over 75% of the frequency samples, their average signal strengths across the 81 frequencies differ by only 0.1dB.

Polarisation settings have great impact on the correlation between signals of different frequencies. The signal correlation observed across the frequency domain shows completely different patterns under different polarisation settings. Explicitly, for co-polarised settings the pattern forms diagonal stripes, whereas for cross-polarised settings the pattern shows chequered boxes – refer to Figure 5 and Figure 6. The correlation-based assessment of signal correlation patterns across different measurement sites confirms that the patterns are not position-specific, but common across the entire measuring regime.

The variations in signal strength and correlation between different polarisation settings was exploited using a hybrid MRC and SC diversity combining scheme which produced an average polarisation diversity gain of 10.6dB.

REFERENCES

- [1] M. Shafi, M. Zhang, A. Moustakas, P. Smith, A. Molisch, F. Tufvesson and S. Simon, "Polarized MIMO channels in 3-D: models, measurements and mutual information," *IEEE Journal on Selected Areas in Communications*, vol. 24, no. 3, pp. 514-527, Mar. 2006.
- [2] R.G. Vaughan, "Polarisation diversity in mobile communications," *IEEE Transactions on Vehicular Technology*, vol. 39, no. 3, pp. 177-186, Jun. 1990.
- [3] S. Kozono, T. Suruhara and M. Sakamoto, "Base station polarization diversity reception for mobile radio," *IEEE Transactions on Vehicular Technology*, vol. 33, no. 4, pp. 301-306, Nov. 1984.
- [4] S. Catreux, P.F. Driessen and L.J. Greenstein, "Simulation results for an interference-limited multiple-input multiple-output cellular system," *IEEE Communications Letters*, vol. 4, no. 11, pp. 334-336, Nov. 2000.
- [5] R.G. Vaughan and J.B. Andersen, "Antenna diversity in mobile communications," *IEEE Transactions on Vehicular Technology*, vol. 36, no. 4, pp. 149-172, Nov. 1987.
- [6] S. Catreux, L.J. Greenstein and V. Erceg, "Some results and insights on the performance gains of MIMO systems," *IEEE Journal on Selected Areas in Communications*, vol. 21, no. 5, pp. 839-847, Jun. 2003.
- [7] C. Oestges, H. Ozcelik and E. Bonek, "On the practical use of analytical MIMO channel models," *Antennas and Propagation Society International Symposium, 2005 IEEE*, vol. 3B, pp. 406-409, 2005.
- [8] J.S. Colburn, Y. Rahmat-Samii, M.A. Jensen and G.J. Pottie, "Evaluation of personal communications dual-antenna handset diversity performance," *IEEE Transactions on Vehicular Technology*, vol. 47, no. 3, pp. 737-746, Aug. 1998.
- [9] T.K.Y. Lo, "Maximum Ratio Transmission," *IEEE Transactions on Communications*, vol. 47, no. 10, Oct. 1999.
- [10] S. Sanayei and A. Nosratinia, "Antenna selection in MIMO systems," *IEEE Communications Magazine*, vol. 42, no. 10, pp. 68-73, Oct. 2004.
- [11] W. Lee and Y. Yeh, "Polarization Diversity System for Mobile Radio," *IEEE Transactions on Communications*, vol. 20, no. 5, pp. 912-923, Oct. 1972.
- [12] J. Valenzuela-Valdes, M. Garcia-Fernandez, A. Martinez-Gonzalez and D. Sanchez-Hernandez, "Evaluation of True Polarization Diversity for MIMO Systems," *IEEE Transactions on Antennas and Propagation*, vol. 57, no. 9, pp. 2746-2755, Sept. 2009.
- [13] H. Ozcelik and C. Oestges, "Some remarkable properties of diagonally correlated MIMO channels," *IEEE Transactions on Vehicular Technology*, vol. 54, no. 6, pp. 2143-2145, Nov. 2005.
- [14] R.U. Nabar, H. Bolcskei, V. Erceg, D. Gesbert and A.J. Paulraj, "Performance of multiantenna signaling techniques in the presence of polarization diversity," *IEEE Transactions on Signal Processing*, vol. 50, no. 10, pp. 2553-2562, Oct. 2002.
- [15] N. Prayongpun and K. Raoof, "Correlation Effects and Channel Capacities for MIMO Polarization Diversity," *Wireless Communications, Networking and Mobile Computing, International Conference on*, vol. 1, no. 4, pp. 22-24, 2006.
- [16] Q.L. Huang and X.W. Shi, "Channel capacity of indoor MIMO systems in the presence of polarization diversity," *2005 Asia-Pacific Microwave Conference Proceedings*, vol. 3, no. 4, pp. 4-7, Dec. 2005.
- [17] C.B. Dietrich, K. Dietze, J.R. Nealy and W.L. Stutzman, "Spatial, polarization, and pattern diversity for wireless handheld terminals," *IEEE Transactions on Antennas and Propagation*, vol. 49, no. 9, pp. 1271-1281, Sep. 2001.
- [18] H.C. Lo, D.B. Lin, T.C. Yang and H.J. Li, "Effect of Polarization on the Correlation and Capacity of Indoor MIMO Channels," *International Journal of Antennas and Propagation*, Article ID 246348, 11 pages, 2012.
- [19] H.J. Li and C.H. Yu, "Correlation properties and capacity of antenna polarization combinations for MIMO radio channel," in *Proceedings of the IEEE International Antennas and Propagation Symposium*, Jun. 2003.
- [20] T. Svantesson, "On capacity and correlation of multi-antenna systems employing multiple polarizations," in *Proceedings of the IEEE Antennas and Propagation Society International Symposium*, Austin, Jun. 2002.
- [21] V. Erceg, P. Soma, D. S. Baum and S. Catreux, "Multiple-input multiple-output fixed wireless radio channel measurements and modeling using dual-polarized antennas at 2.5 GHz," *IEEE Transactions on Wireless Communications*, vol. 3, no. 6, pp. 2288-2298, Nov. 2004.
- [22] V. Erceg, H. Sampath and S. Catreux-Erceg, "Dual-polarization versus single-polarization MIMO channel measurement results and modeling," *IEEE Transactions on Wireless Communications*, vol. 5, no. 1, pp. 28-33, Jan. 2006.
- [23] F. Quitin, C. Oestges, F. Horlin and P.D. Doncker, "Channel Correlation and Cross-Polar Ratio in Multi-Polarized MIMO Channels: Analytical Derivation and Experimental Validation," in *IEEE 68th Vehicular Technology Conference, VTC 2008-Fall*, Calgary, 2008.
- [24] F. Quitin, C. Oestges, F. Horlin and P.D. Doncker, "Polarization measurements and modeling in indoor NLOS environments," *IEEE Transactions on Wireless Communications*, vol. 9, no. 1, pp. 21-25, Jan 2010.
- [25] Y. Konishi, L. Materum, J.I. Takada, I. Ida and Y. Oishi, "Cluster polarization behavior of a MIMO system: Measurement, modeling and statistical validation of the correlation of its channel parameters," in *Personal, Indoor and Mobile Radio Communications, 2009 IEEE 20th International Symposium on*, Tokyo, 2009, pp. 1786-1790.
- [26] V. M. Kolmonen and e. al., "A Dynamic Dual-Link Wideband MIMO Channel Sounder for 5.3 GHz," *IEEE Transactions on Instrumentation and Measurement*, vol. 59, no. 4, pp. 873-883, Apr. 2010.
- [27] "Channel Sounder," [Online]. Available: <http://www.channelsounder.de/ruskchannelsounder.html>. [Accessed May 2015].
- [28] K. Pearson, "Notes on the history of correlation," *Biometrika*, vol. 13, pp. 25-45, 1920, Reprinted in Pearson and Kendall, pp. 185-205, 1970.
- [29] E. Hoong, "Application of Paired t-test and DOE Methodologies on RFID Tag Placement Testing using Free Space Read Distance," in *IEEE International Conference on RFID*, Grapevine, TX, Mar. 2007.
- [30] J. Rice, *Mathematical Statistics and Data Analysis*, Duxbury Press, Apr. 2006.
- [31] A. Boettcher, C. Schneider, M. Narandzic, P. Vary and R.S. Thomae, "Power and delay domain parameters of channel measurements at 2.53 GHz in an urban macro cell scenario," in *IEEE 2010 Proceedings of the Fourth European Conference on Antennas and Propagation (EuCAP)*, Apr. 2010.
- [32] G.S.N. Raju, *Antennas and wave propagation*, Pearson Education India, 2006.
- [33] F. Qureshi, M. Antoniadis and G.V. Eleftheriades, "A compact and low-profile metamaterial ring antenna with vertical polarization," *IEEE Antennas and Wireless Propagation Letters*, vol. 4, pp. 333-336, 2005.
- [34] P. Kyritsi and D.C. Cox, "Propagation characteristics of horizontally and vertically polarized electric fields in an indoor environment: simple model and results," in *IEEE Vehicular Technology Conference*, Vol. 3, pp. 1422-1426, 2001.
- [35] L. Schmitt, G.T.C. Schreyoegg, I. Viering and H. Meyr, "Maximum ratio combining of correlated diversity branches with imperfect channel state information and colored noise," *IEEE 8th International Symposium on Spread Spectrum Techniques and Applications*, pp. 859-863, 2004.



Cheng Fang received the B.S. degree in Computer Science from the University of Oxford, Oxford, UK in 2008 and the PhD degree in wireless communications from the university of Bedfordshire, Luton, UK in 2015. After which he worked as a research associate and visiting lecturer at the University of Bedfordshire.

His research interest includes small cell propagation modelling, MIMO antennas, deterministic propagation modelling, polarisation diversity, Bayesian networks, cryptocurrency and GPUs.



Enjie Liu received the B.S. degree in Computer Science from Northwest University, Xian, China, in 1987, and the PhD degree in Telecommunications from Queen Mary, University of London in 2002.

After the PhD, she worked as Researcher at Nortel Networks Harlow Lab, and Research Fellow at University of Surrey. In 2003, she joined University of Bedfordshire, UK, as Lecturer and she is now Reader in Network Applications. Her current research interests include power management at protocol stack for mobile terminals, small cell propagation modelling, Internet of Things protocols and applications.

Dr. Liu is a Fellow of the Higher Education Academy (UK), she served as a reviewer for several journals, including IEEE Transactions on Vehicular Technology, IEEE Transactions on Wireless Communications, International Journal of Computer Applications in Technology (IJCAT) and European Association for Signal Processing (EURASIP) Journal on Wireless Communications and Networking. She also served as TPC Members, including IEEE Globecom05, IEEE 74th Vehicular Technology Conference and IEEE Wireless Communication & Networking Conference (05-06).



Masood Ur Rehman (SM'16) received the B.Sc. degree in electronics and telecommunication engineering from University of Engineering and Technology, Lahore, Pakistan in 2004 and the M.Sc. and Ph.D. degrees in electronic engineering from Queen Mary University of London, London, UK, in 2006 and 2010, respectively. He worked at Queen Mary University of

London as a postdoctoral research assistant till 2012 before joining the Centre for Wireless Research at University of Bedfordshire, University Square, Luton, UK, as a lecturer.

His research interests include compact antenna design, radio wave propagation and channel characterization, satellite navigation system antennas in cluttered environment, antenna interaction with human body, body-centric wireless networks and sensors, remote health care technology, mmWave and nano communications for body-centric networks and body-to-body communications. He has worked on a number of projects supported by industrial partners and research councils. He has contributed to a patent and authored/co-authored 3 books, 7 book chapters and more than 60 technical articles in leading journals and peer reviewed conferences.

Dr. Ur Rehman is a Fellow of the Higher Education Academy (UK), a member of the IET and part of the technical program committees and organizing committees of several international conferences, workshops and special sessions. He also serves as a reviewer for book publishers, IEEE conferences and leading journals.